Published by Institute of Physics Publishing for SISSA/ISAS
Received: *April 3, 2003*
Accepted: *May 9, 2003*

Global analysis of a supersymmetric Pati-Salam model

Tomáš Blažek,* Stephen F. King and Jonathan K. Parry

Department of Physics and Astronomy, University of Southampton
Southampton, SO17 1BJ, UK
E-mail: Blazek@hep.phys.soton.ac.uk, king@soton.ac.uk, j.parry@hep.phys.soton.ac.uk

Abstract: We perform a complete global phenomenological analysis of a realistic string-inspired model based on the supersymmetric Pati-Salam $\mathrm{SU}(4)\times\mathrm{SU}(2)_L\times\mathrm{SU}(2)_R$ gauge group supplemented by a U(1) family symmetry, and present predictions for all observables including muon $g-2$, $\tau\to\mu\gamma$, and the CHOOZ angle. Our analysis demonstrates the compatibility of such a model with all laboratory data including charged fermion masses and mixing angles, LMA MSW and atmospheric neutrino masses and mixing angles, and $b\to s\gamma$, allowing for small deviations from third family Yukawa unification. We show that in such models the squark and slepton masses may be rather light compared to similar models with exact Yukawa unification.

Keywords: Supersymmetry Phenomenology, GUT, Higgs Physics, Neutrino Physics.

JHEP05(2003)016

*On leave of absence from the Dept. of Theoretical Physics, Comenius Univ., Bratislava, Slovakia

Contents

1. Introduction

The origin of fermion masses and mixing angles represents a challenge faced by theorists for a long time. In the post-SuperKamiokande era this puzzle has become more intriguing than ever before. SuperKamiokande evidence for atmospheric neutrino oscillations [1] has taught us that neutrino masses are non-zero and furthermore that the 23 mixing angle is almost maximal. More recently SNO [2] and KamLAND [3] experimemts have confirmed the matter enhanced Large Mixing Angle(LMA) solution to the solar neutrino problem [4]. In this work we assume that the smallness of neutrino masses can be explained by the see-saw mechanism involving very heavy right-handed neutrino states, and that the see-saw mechanism is implemented using single right-handed neutrino dominance [5] which can explain in a natural way the coexistence of large neutrino mixing angles with a mass hierarchy. It then becomes a flavour problem to fit together the neutrino mass puzzle with the pieces provided by the long-known pattern of quark and charged lepton masses.

The flavour problem cannot be fully addressed without unification. However, unification has its own challenges. These include the unification of gauge couplings and third family Yukawa couplings and the introduction of supersymmetry. It is well known that supersymmetry facilitates gauge coupling unification, stabilises the hierarchy between the high energy scale and the weak scale, and allows a radiative mechanism of electroweak symmetry breaking. Within the natural framework of supersymmetric unification, the larger high energy gauge group in turn increases the predictive power of the theory in the flavour sector, for example by leading to group theoretical mass relations between quark and lepton masses of the same family. Relations between quarks and leptons of different families

JHEP05(2003)016

require an additional family symmetry, however. In this way it becomes possible to address both the flavour problem and the unification problem, within a single framework. Having defined the framework, it is by no means guaranteed that models exist which satisfy all the phenomenological constraints provided by current data, and comply with all the theoretical requirements such as successful electroweak symmetry breaking, and approximate gauge and Yukawa unification, while reproducing the known observables. It is therefore important to know that at least some models exist which satisfy all the constraints, as an existence proof that such a proceedure can be implemented consistently.

In this paper we shall study a particular example of a complete supersymmetric unified model of flavour, based on the Pati-Salam $\mathrm{SU}(4) \times \mathrm{SU}(2)_L \times \mathrm{SU}(2)_R$ gauge group [6] extended by an additional U(1) family symmetry. Accepting minimality as a model building principle this group has the following nice features: it establishes the third family Yukawa unification, places the right-handed neutrinos into non-trivial multiplets and does not introduce unwanted exotic states in the multiplets containing the Standard Model fermions and two Higgs doublets required by its SUSY extension. The Pati-Salam group can emerge from a simple gauge group like SO(10) or $E(6)$. However, from a string theory perspective, it is not necessary in order to achieve unification that there should be a unified field theory based on a simple group. A partially unified gauge group can equally well emerge directly from string theory, and in the case of the Pati-Salam gauge group this possibility has been explored extensively both in the case of weakly coupled fermionic string theories [7] and in the case of type I strings with D-branes [8].

Although models based on the Pati-Salam gauge group have been extensively examined, there is currently no complete up to date phenomenological study of this model in the literature. For instance [9] investigated constraints from Lepton Flavour Violation(LFV) in a Pati-Salam model with small neutrino mixing angles. Subsequently a Pati-Salam model was proposed [10], using single right-handed neutrino dominance [5] to achieve naturally large neutrino mixing angles, but the question of LFV was not readdressed and it was later shown [11] that the $\mu \to e\gamma$ branching ratio is too large. Moreover, only the negative μ parameter was considered in [10, 12] which is currently disfavoured by the muon $g-2$. In other works such as [13] and [14] the neutrino sector is absent all together. The complete lepton sector is studied in great detail in a global analysis in [11], but the quark mass matrices used [10] were obtained for the opposite sign of μ, and the analysis gives imperfect fits for the branching ratio $BR(b \to s\gamma)$ or b quark mass m_b which both get potentially significant contributions from SUSY loops proportional to μ. To summarise, a completely phenomenologically acceptable supersymmetric Pati-Salam model does not currently exist in the literature. This illustrates the broader point that while many models exist in the literature, it is less common for the analysis of any such model to be complete.

In this paper, then, we shall construct a "4221" model, following the approach of [10], and demonstrate its phenomenological viability. The model has approximate third family Yukawa unification perturbed by higher order terms and assumes non-universal soft Higgs masses. To demonstrate the viability of such a model, we perform a top down global analysis of the parameter space carried out on 24 observables. In the leptonic sector the observables include the muon $g-2$ and solar and atmospheric neutrino data. A complete list of observables and their σ values, which are used to calculate the χ^2 function can be found in table 2. In the analysis we ensure that the upper limits on the branching ratio for the lepton flavour violating processes $\tau \to \mu\gamma$, $\mu \to e\gamma$ and $\tau \to e\gamma$ are not exceeded as well as the limit on the 13 neutrino mixing angle. In addition to this an experimental lower bound on each sparticle mass was imposed. In particular, the most constraining are: the LEP limits on the charged SUSY masses ($m_{\tilde{\chi}^\pm}, m_{\tilde{\tau}} > 105\,\text{GeV}$), the CDF limit on the mass of the CP odd Higgs state ($m_{A^0} > 105\text{-}110\,\text{GeV}$, valid for $\tan\beta \approx 50$) [15], and the requirement that the lightest SUSY particle should be neutral.

Having constructed the model and demonstrated its phenomenological viability, we then discuss the following three aspects of the model in more detail:

- The first such aspect, as first pointed out in [11], is lepton flavour violation arising from the large 23 neutrino mixing through a neutrino Yukawa texture of the form

$$Y^{\nu}_{LR} \sim \begin{pmatrix} 0 & 0 & 0 \\ 0 & 0 & 1 \\ 0 & 0 & 1 \end{pmatrix}. \tag{1.1}$$

  Due to large $\tan\beta$ additional features emerge when studying correlations among observables like $\text{BR}(b \to s\gamma)$, $\text{BR}(\tau \to \mu\gamma)$ and muon $g-2$. Most notably, two distinct minima are found with similar χ^2 values for the best fits. These conclusions are new since study [11] did not investigate a complete model and all other previous works did not involve global analysis.

- The preference for positive μ, given by the sign of the muon $g-2$ discrepancy, implies positive gluino corrections to m_b thus leading to difficulties in obtaining $t-b-\tau$ Yukawa unification. Hence a second focus of the present work is to study the required deviation from third family Yukawa unification in the best fits.[1]

- Thirdly we focus on the effects of future experimental advances, in the form of direct Higgs searches, a lepton flavour violating $\tau \to \mu\gamma$ measurement and a refinement of the muon $g-2$ discepancy, upon our global fits, indicating how further experimental progress in these areas will constrain the parameter space of the model.

The remainder of the paper is layed out as follows. Section 2 briefly reviews our construction of a string-inspired Pati-Salam model. Section 3 contains a brief description of the numerical technique used in the analysis. A discussion of our main results can be found in section 4, with concluding remarks in section 5.

2. The model

The model considered in this paper is based on the Pati-Salam gauge group [6], supplemented by a U(1) family symmetry,

$$\text{SU}(4) \times \text{SU}(2)_L \times \text{SU}(2)_R \times \text{U}(1) \tag{2.1}$$

[1] This was also recently studied from a somewhat different point of view in [13].

The left-handed quarks and leptons are accommodated in the following representations,

$$F^{i\alpha a} = (4,2,1) = \begin{pmatrix} u^R & u^B & u^G & \nu \\ d^R & d^B & d^G & e^- \end{pmatrix}^i \tag{2.2}$$

$$\overline{F}^i_{x\alpha} = (\bar{4},1,\bar{2}) = \begin{pmatrix} \bar{d}^R & \bar{d}^B & \bar{d}^G & e^+ \\ \bar{u}^R & \bar{u}^B & \bar{u}^G & \bar{\nu} \end{pmatrix}^i \tag{2.3}$$

where $\alpha = 1, \ldots, 4$ is an SU(4) index, $a, x = 1, 2$ are $\mathrm{SU}(2)_{L,R}$ indices, and $i = 1, \ldots, 3$ is a family index. The Higgs fields are contained in the following representations,

$$h^x_a = (1,\bar{2},2) = \begin{pmatrix} {h_2}^+ & {h_1}^0 \\ {h_2}^0 & {h_1}^- \end{pmatrix} \tag{2.4}$$

(where h_1 and h_2 are the low energy Higgs superfields associated with the MSSM.) The two heavy Higgs representations are [7]

$$H^{\alpha b} = (4,1,2) = \begin{pmatrix} u^R_H & u^B_H & u^G_H & \nu_H \\ d^R_H & d^B_H & d^G_H & e^-_H \end{pmatrix} \tag{2.5}$$

and

$$\overline{H}_{\alpha x} = (\bar{4},1,\bar{2}) = \begin{pmatrix} \bar{d}^R_H & \bar{d}^B_H & \bar{d}^G_H & e^+_H \\ \bar{u}^R_H & \bar{u}^B_H & \bar{u}^G_H & \bar{\nu}_H \end{pmatrix}. \tag{2.6}$$

The Higgs fields are assumed to develop VEVs,

$$\langle H \rangle \equiv \langle \nu_H \rangle \sim M_{\mathrm{GUT}}\,, \qquad \langle \overline{H} \rangle \equiv \langle \bar{\nu}_H \rangle \sim M_{\mathrm{GUT}} \tag{2.7}$$

leading to the symmetry breaking at M_{GUT}

$$\mathrm{SU}(4) \otimes \mathrm{SU}(2)_L \otimes \mathrm{SU}(2)_R \longrightarrow \mathrm{SU}(3)_C \otimes \mathrm{SU}(2)_L \otimes \mathrm{U}(1)_Y \tag{2.8}$$

in the usual notation. Under the symmetry breaking in eq. (2.8), the Higgs field h in eq. (2.4) splits into two Higgs doublets h_1, h_2 whose neutral components subsequently develop weak scale VEVs,

$$\langle h^0_1 \rangle = v_1\,, \qquad \langle h^0_2 \rangle = v_2 \tag{2.9}$$

with $\tan\beta \equiv v_2/v_1$.

To construct the quark and lepton mass matrices we make use of non-renormalisable operators [16] of the form:

$$\text{(i)} \qquad (F^i\overline{F}^j)h\left(\frac{H\overline{H}}{M^2}\right)^n \left(\frac{\theta}{M}\right)^{p_{ij}} \tag{2.10}$$

$$\text{(ii)} \qquad (\overline{F}^i\overline{F}^j)\left(\frac{HH}{M^2}\right)\left(\frac{H\overline{H}}{M^2}\right)^m \left(\frac{\theta}{M}\right)^{q_{ij}}\,. \tag{2.11}$$

The θ fields are Pati-Salam singlets which carry U(1) family charge and develop VEVs which break the U(1) family symmetry. They are required to be present in the operators above to balance the charge of the invariant operators. After the H and θ fields acquire VEVs, they generate a hierarchy in (i) effective Yukawa couplings and (ii) Majorana masses. These operators are assumed to originate from additional interactions at the scale $M > M_{\rm GUT}$. The value of the powers p_{ij} and q_{ij} are determined by the assignment of U(1) charges, with $X_\theta = -1$ then $p_{ij} = (X_{F^i} + X_{\overline{F}^j} + X_h)$ and $q_{ij} = (X_{\overline{F}^i} + X_{\overline{F}^j} + X_h)$.

The contribution to the third family Yukawa coupling is assumed to be only from the renormalisable operator with $n = p = 0$ leading to Yukawa unification. The contribution of an operator, with a given power n, to the matrices $Y_{f=u,d,\nu,e}$, M_{RR} is determined by the relevant Clebsch factors coming from the gauge contractions within that operator. A list of Clebsch factors for all $n = 1$ operators can be found in the appendix of [10]. These Clebsch factors give zeros for some matrices and not for others, hence a choice of operators can be made such that a large 23 entry can be given to Y_ν and not $Y_{u,d,e}$. We shall write,

$$\delta = \frac{\langle H\rangle\langle\overline{H}\rangle}{M^2} = 0.22\,, \qquad \epsilon = \frac{\langle\theta\rangle}{M^2} = 0.22\,, \tag{2.12}$$

then we can identify δ with mass splitting within generations and ϵ with splitting between generations.

Our choice of U(1) charges are as in [10], and can be summarised as $X_{F^i} = (1,0,0)$, $X_{\overline{F}^i} = (4,2,0)$, $X_h = 0$, $X_H = 0$ and $X_{\overline{H}} = 0$. This fixes the powers of ϵ in each entry of the Yukawa matrix, but does not specify the complete operator. The Yukawa couplings are specified by the choice of operators,

$$Y_f(M_{\rm GUT}) = \begin{pmatrix} (a_{11}\mathcal{O}^R + a''_{11}\mathcal{O}''^V)\epsilon^5 & (a_{12}\mathcal{O}^I + a'_{12}\mathcal{O}'^F)\epsilon^3 & (a'_{13}\mathcal{O}'^c)\epsilon \\ (a_{21}\mathcal{O}^G)\epsilon^4 & (a_{22}\mathcal{O}^W + a'_{22}\mathcal{O}'^S)\epsilon^2 & (a_{23}\mathcal{O}^I + a'_{23}\mathcal{O}'^W) \\ (a_{31}\mathcal{O}^R)\epsilon^4 & (a_{32}\mathcal{O}^M + a'_{32}\mathcal{O}'^K)\epsilon^2 & a_{33} \end{pmatrix} \tag{2.13}$$

The operators are defined in [10], although the selection of operators here is different from that paper. The notation is such that $\mathcal{O}$, $\mathcal{O}'$ and $\mathcal{O}''$ are $n = 1$, $n = 2$ and (highly small) $n = 3$ operators respectively where n refers to the powers of $(H\overline{H})$, thus[2]

$$\mathcal{O} \sim (H\overline{H}) \sim \delta\,, \qquad \mathcal{O}' \sim (H\overline{H})^2 \sim \delta^2\,, \qquad \mathcal{O}'' \sim (H\overline{H})^3 \sim \delta^3\,. \tag{2.14}$$

The order unity coefficients a_{ij}, a'_{ij}, a''_{ij} multiply the operators $\mathcal{O}$, $\mathcal{O}'$, $\mathcal{O}''$ in the ij position. The Majorana operators are assumed to arise from an $m = 0$ operator in the 33 position and $m = 1$ operators elsewhere. The operator choice in eq. (2.13) leads to the quark and lepton mass matrices in table 1. For example the Clebsch coeficients from the leading $\mathcal{O}^W$ operator in the 22 positon gives the ratio $0:1:3$ in the $Y_{U,D,E}$ matrices. This ratio along with subleading corrections provides the correct $m_c : m_s : m_\mu$ ratio.

In the neutrino sector the matrices in table 1 satisfy the condition of sequential dominance [5] in which a neutrino mass hierarchy naturally results with the dominant third right-handed neutrino being mainly responsible for the atmospheric neutrino mass, and the sub-dominant second right-handed neutrino being mainly responsible for the solar neutrino mass. The atmospheric mixing angle is then determined approximately as a ratio

[2]The $n = 3$ operators can, to a very good approximation, be neglected. Their inclusion here serves only to fill the 11 entries of the $Y_{u,\nu}$ Yukawa matrices, thereby ensuring (for example) that the up quark is given a very small mass.

$$
\begin{aligned}
Y_u(M_{\mathrm{GUT}}) &= \begin{pmatrix} \sqrt{2}\, a''_{11}\delta^3\epsilon^5 & \sqrt{2}\, a'_{12}\delta^2\epsilon^3 & \frac{2}{\sqrt{5}}\, a'_{13}\delta^2\epsilon \\ 0 & \frac{8}{5\sqrt{5}}\, a'_{22}\delta^2\epsilon^2 & 0 \\ 0 & \frac{8}{5}\, a'_{32}\delta^2\epsilon^2 & r_t a_{33} \end{pmatrix} \\
Y_d(M_{\mathrm{GUT}}) &= \begin{pmatrix} \frac{8}{5}\, a_{11}\delta\epsilon^5 & -\sqrt{2}\, a'_{12}\delta^2\epsilon^3 & \frac{4}{\sqrt{5}}\, a'_{13}\delta^2\epsilon \\ \frac{2}{\sqrt{5}}\, a_{21}\delta\epsilon^4 & \sqrt{\frac{2}{5}}\, a_{22}\delta\epsilon^2 + \frac{16}{5\sqrt{5}}\, a'_{22}\delta^2\epsilon^2 & \sqrt{\frac{2}{5}}\, a'_{23}\delta^2 \\ \frac{8}{5}\, a_{31}\delta\epsilon^5 & \sqrt{2}\, a_{32}\delta\epsilon^2 & r_b a_{33} \end{pmatrix} \\
Y_e(M_{\mathrm{GUT}}) &= \begin{pmatrix} \frac{6}{5}\, a_{11}\delta\epsilon^5 & 0 & 0 \\ \frac{4}{\sqrt{5}}\, a_{21}\delta\epsilon^4 & -3\sqrt{\frac{2}{5}}\, a_{22}\delta\epsilon^2 + \frac{12}{5\sqrt{5}}\, a'_{22}\delta^2\epsilon^2 & -3\sqrt{\frac{2}{5}}\, a'_{23}\delta^2 \\ \frac{6}{5}\, a_{31}\delta\epsilon^5 & \sqrt{2}\, a_{32}\delta\epsilon^2 & a_{33} \end{pmatrix} \\
Y_\nu(M_{\mathrm{GUT}}) &= \begin{pmatrix} \sqrt{2}\, a''_{11}\delta^3\epsilon^5 & 2\, a_{12}\delta\epsilon^3 & 0 \\ 0 & \frac{6}{5\sqrt{5}}\, a'_{22}\delta^2\epsilon^2 & 2\, a_{23}\delta \\ 0 & \frac{6}{5}\, a'_{32}\delta^2\epsilon^2 & r_\nu a_{33} \end{pmatrix} \\
\frac{M_{RR}(M_{\mathrm{GUT}})}{M_R} &= \begin{pmatrix} A_{11}\delta\epsilon^8 & A_{12}\delta\epsilon^6 & A_{13}\delta\epsilon^4 \\ A_{12}\delta\epsilon^6 & A_{22}\delta\epsilon^4 & A_{23}\delta\epsilon^2 \\ A_{13}\delta\epsilon^4 & A_{23}\delta\epsilon^2 & A_{33} \end{pmatrix}
\end{aligned}
$$

Table 1: The quark and lepton Yukawa matrices and neutrino Majorana mass matrix as used in the analysis. In our numerical analysis we set $M_R = 3 \cdot 10^{14}$ GeV. The Yukawa matrices follow from eq. (2.13) and the Clebsch factors arising from each operator are shown numerically above. Clebsch zeroes play an important part in suppressing the leading operator contribution in a particular element of the matrix, or in simply giving a zero if all the operators are suppressed. The Clebsch coefficients in the Majorana sector are set equal to unity, with A_{ij} being independent order unity coefficients.

of $Y_\nu^{23} : Y_\nu^{33}$, and the solar mixing angle is determined by a ratio of Y_ν^{12} to a linear combination of Y_ν^{22} and Y_ν^{32}, while the CHOOZ angle is determined by a more complicated formula [17]. Note that the dominant right-handed neutrino in this model is the heaviest one, corresponding to heavy sequential dominance (HSD) and LFV has been considered in general in this class of models [18].

In the previous analysis [11] the matrix elements, Y_e^{12}, $Y_{e,\nu}^{13}$ were suppressed artificially to keep $BR(\mu \to e\gamma)$ within its experimental limit without substantially changing the predictions of fermion masses and mixings. In this new analysis we have built this suppression into the model with our new choice of operators, whose Clebsch coefficients give zeros in the desired matrix elements as can be seen in table 1. This can be understood analytically from [18].

The subleading operators in the 33 position are not shown explicitly, but are expected to lead to significant deviations from exact Yukawa unification. This effect is parametrised by the ratios

$$
r_t \equiv \frac{Y_u(M_{\mathrm{GUT}})_{33}}{Y_e(M_{\mathrm{GUT}})_{33}}\,, \qquad r_b \equiv \frac{Y_d(M_{\mathrm{GUT}})_{33}}{Y_e(M_{\mathrm{GUT}})_{33}}\,, \qquad r_\nu \equiv \frac{Y_\nu(M_{\mathrm{GUT}})_{33}}{Y_e(M_{\mathrm{GUT}})_{33}}\,. \tag{2.15}
$$

JHEP05(2003)016

3. Numerical procedure

In our numerical analysis we have adopted a complete top-down approach [19]. At the GUT scale the MSSM gauge couplings are related to the GUT scale couplings as $\alpha_{2L} = \alpha_1 = \alpha_{\rm GUT}$ and $\alpha_3 = \alpha_{\rm GUT}(1+\epsilon_3)$, where ϵ_3 sums up the effects of GUT scale threshold corrections. The particular choice of the Yukawa couplings, table 1, follows from the higher dimensional operators in eq. (2.13) as the latter are matched to the MSSM lagrangian. The parameters

$$\begin{aligned} &M_{\rm GUT}\,,\ \alpha_{\rm GUT}\,,\ \epsilon_3\,,\ \delta\,,\ \epsilon,\ a\text{'s and } A\text{'s}\,,\ r_t\,,\ r_b\,,\ r_\nu\,, \\ &M_{1/2}\,,\ A_0\,,\ \mu\,,\ B\mu\,,\ m_F^2\,,\ m_{\overline{F}}^2,\ m_h^2 \text{ and } D^2 \end{aligned} \tag{3.1}$$

are then defined by the boundary conditions at the GUT scale. They parametrise the imprint of a complete Pati-Salam theory together with the SUSY sector (second line) on the MSSM and stand for the input in case this theory is not fully known. In the SUSY sector, the soft SUSY breaking parameters are for simplicity introduced at the same scale. The gaugino masses are assumed universal (equal to $M_{1/2}$) and so do the trilinear couplings: $A_i = A_0\, Y_i$, for $i = u,\ d,\ e,\ \nu$. The soft scalar masses of the MSSM superfields include the D terms from the breaking of the Pati-Salam gauge group [12]

$$\begin{aligned} m_Q^2 &= m_F^2 + g_4^2\, D^2 \\ m_{u_R}^2 &= m_{\overline{F}}^2 - (g_4^2 - 2g_{2R}^2)\, D^2 \\ m_{d_R}^2 &= m_{\overline{F}}^2 - (g_4^2 + 2g_{2R}^2)\, D^2 \\ m_L^2 &= m_F^2 - 3g_4^2\, D^2 \\ m_{e_R}^2 &= m_{\overline{F}}^2 + (3g_4^2 - 2g_{2R}^2)\, D^2 \\ m_{\nu_R}^2 &= m_{\overline{F}}^2 + (3g_4^2 + 2g_{2R}^2)\, D^2 \\ m_{H_u}^2 &= m_h^2 - 2g_{2R}^2\, D^2 \\ m_{H_d}^2 &= m_h^2 + 2g_{2R}^2\, D^2\,. \end{aligned} \tag{3.2}$$

As $D^2 = \frac{1}{8}\left(|\overline{H}_\nu|^2 - |H_\nu|^2\right)$ [12] it is possible for this quantity to be both positive and negative.

We now describe minor simplifications to the input in (3.1) which were assumed in the actual numerical analysis. We have kept equality between the two order parameters δ and ϵ as in eq. (2.12) and the soft SUSY breaking scalar masses m_F and $m_{\overline{F}}$ have been held equal to each other as well. Furthermore we exploited the fact that determining $\mu(M_{\rm GUT})$ and $B\mu$ at the GUT scale is equivalent to determining the low energy values $\mu(M_Z)$ and $\tan\beta$, respectively. Thus instead of (3.1) our numerical analysis uses

$$\begin{aligned} &M_{\rm GUT}\,,\ \alpha_{\rm GUT}\,,\ \epsilon_3\,,\ \delta\,,\ a\text{'s and } A\text{'s}\,,\ r_t\,,\ r_b\,,\ r_\nu\,, \\ &M_{1/2}\,,\ A_0\,,\ \mu(M_Z)\,,\ \tan\beta\,,\ m_F^2\,,\ m_h^2 \text{ and } D^2 \end{aligned} \tag{3.3}$$

as input parameters. The top down approach implies that we can freely vary or hold fixed any one of them and then investigate the fit properties. This is one of the advantages of doing the analysis top down. For example, in more traditional bottom up approaches it is difficult to control the size of the dimensionless GUT scale parameters. One usually sets up a sample of randomly scattered points and then searches through it to identify a sub-sample with physically interesting GUT scale properties. In our case we can set up the interesting GUT relations explicitly right at the start — as we have done for instance in section 4.3 where the fits with r_b and r_t approaching unity are studied.

We note that taking advantage of the top-down approach we kept $\delta = 0.22$, $r_\nu = 1$, $A_0 = 0$ and $\tan\beta = 50$ fixed throughout the analysis. This effectively increases the degrees of freedom of the global analysis and can provide a reference point if further analysis is required in the future. We also kept the μ parameter at scale M_Z fixed to two different values as is explained below.

Observable	Mean	σ_i
α_{EM}	1/137.036	$7.30 \cdot 10^{-6}$
G_μ	$1.16639 \cdot 10^{-5}$	$1.12 \cdot 10^{-7}$
$\alpha_s(M_Z)$	0.1181	0.0020
M_t	174.3	5.1
$m_b(m_b)$	4.20	0.20
$M_b - M_c$	3.4	0.2
$m_s(2\,\mathrm{GeV})$	0.110	0.035
$(m_d^2 - m_u^2)/m_s^2$	$2.03 \cdot 10^{-3}$	$2.0 \cdot 10^{-4}$
m_d/m_s	0.05	0.015
M_τ	1.777	$1.8 \cdot 10^{-3}$
M_μ	0.106	$1.1 \cdot 10^{-4}$
M_e	$5.11 \cdot 10^{-4}$	$5.1 \cdot 10^{-7}$
$\lvert V_{us}\rvert$	0.2196	0.0023
$\lvert V_{cb}\rvert$	0.0402	0.003
$\lvert V_{ub}\rvert/\lvert V_{cb}\rvert$	0.09	0.02
M_Z	91.1882	0.091
M_W	80.419	0.08
ρ_{NEW}	-0.0002	0.0011
$BR(b \to s\gamma)$	$3.47 \cdot 10^{-4}$	$0.45 \cdot 10^{-4}$
$\delta a_{\mu\ NEW}$	$34.7.6 \cdot 10^{-10}$	$11 \cdot 10^{-10}$
Δm^2_{rmATM}	$2.5 \cdot 10^{-3}$	$0.8 \cdot 10^{-3}$
$\sin^2 2\theta_{rmATM}$	0.99	0.06
$\Delta m^2_{\mathrm{SOL}}$	$7.0 \cdot 10^{-5}$	$3 \cdot 10^{-5}$
$\sin^2 2\theta_{\mathrm{SOL}}$	0.8	0.09

Table 2: Table of observables and σ values which are used to calculate the χ^2 that enables best fit regions to be determined via minimisation.

Two-loop RGEs for the dimensionless couplings and one-loop RGEs for the dimensionful couplings were used to run all couplings down to the scale M_{3R} where the heaviest right-handed neutrino decoupled from the RGEs. Similar steps were taken for the lighter M_{2R} and M_{1R} scales, and finally with all three right-handed neutrinos decoupled the solutions for the MSSM couplings and spectra were computed at the Z scale. This includes full one loop SUSY threshold corrections to the fermion mass matrices and all Higgs masses while the sparticle masses are obtained at tree level.

m_h and D in eqs. (3.2) were varied to optimise radiative electroweak symmetry breaking (REWSB), which was checked at one loop with the leading m_t^4 and m_b^4 corrections included following the effective potential method in [20]. We note that as $\tan\beta$ determines the Higgs bilinear parameter $B\mu$, there is a redundancy in our procedure since two input parameters, m_h and D, determine one condition for the Higgs VEV of 246 GeV. This approach enabled us to control the μ parameter and we explored regions with μ low ($\mu = 120\,\mathrm{GeV}$) and high ($\mu = 300\,\mathrm{GeV}$).[3]

[3]For $\tan\beta$ as large as 50, $\mu \gg 300\,\mathrm{GeV}$ leads to too large SUSY threshold corrections to the masses of the third generation fermions τ and b unless the sparticles in the loop have masses well above the 1 TeV region [21, 19].

An experimental lower bound on each sparticle mass was imposed. In particular, the most constraining are: the LEP limits on the charged SUSY masses ($m_{\tilde{\chi}^{\pm}}, m_{\tilde{\tau}} > 105\,\mathrm{GeV}$), the CDF limit on the mass of the CP odd Higgs state ($m_{A^0} > 105$-$110\,\mathrm{GeV}$, valid for $\tan\beta \approx 50$) [15], and the requirement that the lightest SUSY particle should be neutral. Finally, the χ^2 function $\sum(X_i^{th} - X_i^{exp})^2/\sigma_i^2)$ is evaluated based on the agreement between the theoretical predictions and 24 experimental observables collected in table 2. In addition to the constraints listed above and in [11], we make a full analysis of the quark sector mass and mixings, in particular we have included the important constraint set by BR($b \to s\gamma$).

4. Results and discussion

The numerical results from the global analysis are presented in the form of contour plots in the $(m_F, M_{1/2})$ plane and are produced for two different values of the mu parameter $\mu = 120\,\mathrm{GeV}$ and $\mu = 300\,\mathrm{GeV}$. Before we address the details we would like to discuss two different viewpoints of our analysis, namely the flavour sector on the one hand and the unification sector of the other hand. In our discussion we would like to distinguish between the two viewpoints. The main distinction is that in the MSSM analysis the flavour parameters a_{ij} (with the exception of a_{33}) and A_{ij} can be considered fixed at unity or at a value of order unity. Up to a_{33} which enters the large Yukawa couplings their exact values do not affect the fit of the SUSY spectra or SUSY-related observables like the muon $g-2$ or branching ratio $b \to s\gamma$. They neither perturb gauge coupling unification nor change the running of the large Yukawa couplings. This means that the discussion of our results is naturally split into a part dealing with the flavour structure of the Pati-Salam model where the variation of the coefficients of the higher dimensional operators matters, and a part where the MSSM analysis is presented and the conclusions do not depend on the variation of the a and A parameters (up to a_{33}).

Concerning the flavour sector, our results can be used to show how well the model, i.e. the set of higher dimensional operators specified by eq. (2.13), describes the observed fermion masses and mixings. Taking this viewpoint all parameters listed in (3.3) represent the input of the analysis. The results in either of the four panels in figure 1 show that the model gives a very good agreement with the data. The minimum of the total χ^2 is less than unity obtained for $\mu = 120\,\mathrm{GeV}$ in the upper left panel. This means that it is possible to fit every observable to better than a $1\,\sigma$ accuracy.

Concerning the unification sector, the conclusions are much stronger as much fewer number of the input parameters enters effectively after the a's and A's decouple from the analysis. Indeed, the set of the effective input parameters in this sector is reduced to

$$\begin{aligned} &M_{\mathrm{GUT}}\,,\ \alpha_{\mathrm{GUT}}\,,\ \epsilon_3\,,\ a_{33}\,,\ r_t\,,\ r_b\,, \\ &M_{1/2}\,,\ m_F^2\,,\ m_h^2 \text{ and } D^2\,. \end{aligned} \tag{4.1}$$

With this input the low energy Higgs and SUSY spectra are determined. The conventional present-day observables include α_{EM}, G_μ, $\alpha_s(M_Z)$, M_t, $m_b(m_b)$, M_τ, M_Z, M_W, ρ_{NEW}, $BR(b \to s\gamma)$ and δa_μ. The a_{ij} and A_{ij} input parameters are all of order one and their exact values are always adjusted to fit the first two generation masses and mixings well while these variations do not affect the fit of the observables listed above.

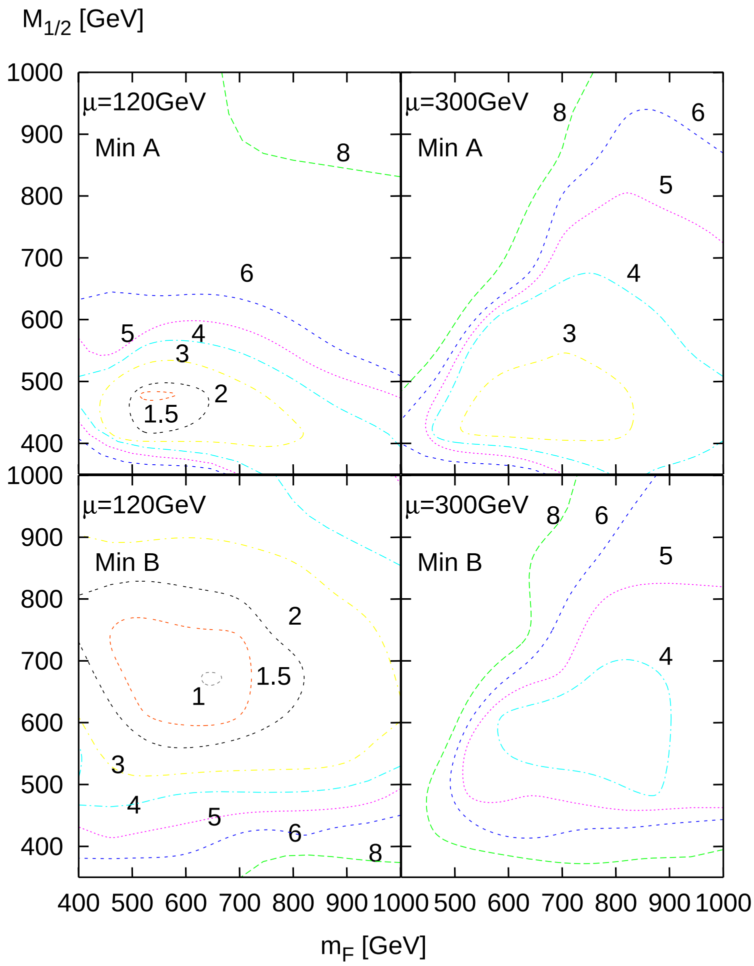

Figure 1: χ^2 contour plot in the plane of $(m_F, M_{1/2})$. The four plots, are obtained from the two minima, minimum A and minimum B with μ = 120 and 300 GeV as labelled. All points in the top left corner with approximately $M_{1/2} > 700$ GeV and $m_F > 700$ GeV are unphysical due to the lightest stau becoming the LSP.

We study many details of the MSSM analysis, in particular the dependence of the fit on m_F^2 and $M_{1/2}$, best fit results for muon $g-2$, and $BR(\tau \to \mu\gamma)$ predictions. The numerical results also contain studies of a deviation from Yukawa unification and a future measurement of $BR(\tau \to \mu\gamma)$. The effect of a change to the present muon $g-2$ discrepancy was studied and also the effect of future direct Higgs searches, the results of which can also be found at the end of the paper.

From our global analysis we found that there are two χ^2 minima as shown in figure 1. In this model there are two conditions and three free variables, m_h^2, D^2, and $B\mu$, for electroweak symmetry breaking to be achieved. The two minima hence are independent solutions to these conditions. Minimum A has D^2 negative and smaller m_h, $B\mu$. Minimum B on the other hand has D^2 positive and larger m_h, $B\mu$. The relative size of $B\mu$ results in a different Higgs spectrum, particularly the CP odd pseudoscalar Higgs, A^0, which will be lighter for minimum A and heavier for minimum B. The difference between the

Inputs				
	$\mu = 120$ **GeV**		$\mu = 300$ **GeV**	
	Min A	Min B	Min A	Min B
$M_{1/2}$	450	650	450	650
m_F	500	650	500	650
μ	120	120	300	300
D^2	$-6.4 \cdot 10^4$	$17 \cdot 10^4$	$-10 \cdot 10^4$	$13 \cdot 10^4$
m_h^2	$6 \cdot 10^5$	$16 \cdot 10^5$	$4.5 \cdot 10^5$	$14 \cdot 10^5$
r_t	1.01	1.07	1.03	1.02
r_b	0.75	0.72	0.66	0.64
a_{33}	0.55	0.55	0.55	0.56
a_{11}	-0.93	-0.92	-0.92	-0.93
a_{12}	0.20	0.33	0.31	0.30
a_{21}	1.67	1.67	1.67	1.75
a_{22}	1.13	1.12	1.13	1.13
a_{23}	0.98	0.89	1.05	0.85
a_{31}	-0.20	-0.21	-0.20	-0.28
a_{32}	2.18	2.08	2.32	2.53
a'_{12}	0.77	0.77	0.71	0.71
a'_{13}	0.60	0.53	0.46	0.46
a'_{22}	0.66	0.66	0.64	0.62
a'_{23}	0.41	0.40	0.36	0.36
a'_{32}	1.16	1.80	1.56	1.72
a''_{11}	0.32	0.278	0.20	0.23
A_{11}	0.63	0.94	0.63	0.94
A_{12}	0.74	0.48	0.69	0.52
A_{13}	1.75	2.10	1.73	2.04
A_{22}	0.97	0.52	0.93	0.55
A_{23}	2.49	1.79	2.23	1.91
A_{33}	1.97	1.88	1.97	1.88

Table 3: Tables of inputs for the best fit points for each of the global χ^2 minima with $\mu = 120$ and 300 GeV.

sign of D^2, which contributes to the soft scalar masses as shown in eq. (26), means that minimum B will have lighter right squarks and left sleptons, along with heavier left squarks and right sleptons, than minimum A. This difference in sign of D^2 has some interesting phenomenological consequences for the two minima which will now be discussed.

The upper and lower plots shown in figure 1, display the χ^2 contours for these two minima. Each of the figures display results for both $\mu = 120$ and 300 GeV in the relative left and right positions. The contours in figure 1 are bounded from the lower m_F region due to the lightest stau becoming the LSP and from the lower $M_{1/2}$ region due to an increasing χ^2 penalty coming from $BR(b \to s\gamma)$.

JHEP05(2003)016

Outputs				
	$\mu = 120$ **GeV**		$\mu = 300$ **GeV**	
	Min A	Min B	Min A	Min B
m_{A^0}	102	818	102	822
m_{h^0}	106	114	106	114
m_{H^0}	112	891	113	888
m_{H^+}	136	861	135	861
M_1	186	270	186	271
M_2	371	537	371	537
M_3	1175	1671	1175	1671
$M_{\chi_1^+}$	114	117	272	290
$M_{\chi_2^+}$	390	549	408	554
$M_{\tilde{N}_1}$	98	107	179	249
$M_{\tilde{N}_2}$	130	127	277	305
$M_{\tilde{N}_3}$	198	278	307	311
$M_{\tilde{N}_4}$	390	549	408	554
$M_{\tilde{Q}_{1,2}}$	1166	1679	1159	1673
$M_{\tilde{Q}_3}$	979	1345	960	1356
$M_{\tilde{U}_{1,2}}$	1131	1623	1124	1617
$M_{\tilde{U}_3}$	798	1147	805	1160
$M_{\tilde{D}_{1,2}}$	1182	1510	1204	1529
$M_{\tilde{D}_3}$	923	1192	1044	1251
$M_{\tilde{L}_1}$	673	611	715	656
$M_{\tilde{L}_2}$	665	595	707	644
$M_{\tilde{L}_3}$	580	334	638	425
$M_{\tilde{E}_1}$	496	766	473	752
$M_{\tilde{E}_2}$	495	765	473	751
$M_{\tilde{E}_3}$	201	370	188	325
$\tau \to \mu\gamma$	$2 \cdot 10^{-7}$	$3 \cdot 10^{-6}$	$8 \cdot 10^{-8}$	$5 \cdot 10^{-7}$
$\tau \to e\gamma$	$1 \cdot 10^{-14}$	$3 \cdot 10^{-13}$	$6 \cdot 10^{-15}$	$5 \cdot 10^{-14}$
$\mu \to e\gamma$	$3 \cdot 10^{-14}$	$1 \cdot 10^{-13}$	$1 \cdot 10^{-14}$	$3 \cdot 10^{-14}$
$\sin\theta_{13}$	0.053	0.078	0.037	0.10
$\sin(\beta-\alpha)$	0.22	1.0	0.15	1.0
$\cos(\beta-\alpha)$	-0.98	0.0	-0.99	0.0

Table 4: Tables of outputs for the best fit points for each of the global χ^2 minima with $\mu = 120$ and 300 GeV. The input parameters are as defined in table 3.

The upper minima of figure 1, Minima A, have a preferred region in the lower $(m_F, M_{1/2})$ plane, with $M_{1/2} = 400 - 500$ GeV and $m_F = 500 - 700$ GeV. The lower minima of figure 1, Minima B, have their preferred region nearer $M_{1/2} = 550 - 650$ GeV and $m_F = 600 - 800$ GeV. A list of inputs and outputs for the best fit point in each minimum can be found in tables 3 and 4. The Higgs masses and CP even Higgs mixings found for minimum A in table 4 are discussed in detail in section 4.4.

JHEP05(2003)016

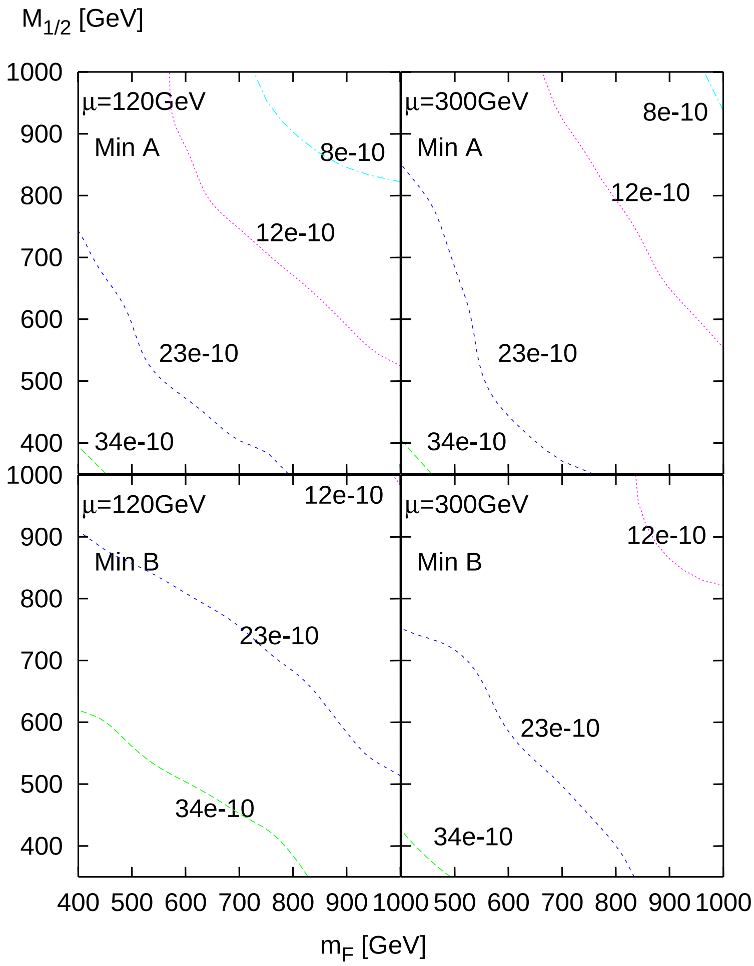

Figure 2: Muon $g-2$ contour plot in the plane of $(m_F, M_{1/2})$. The four plots, are obtained from the two minima, minimum A and minimum B with $\mu = 120$ and $300\,\text{GeV}$ as labelled. All points to the left of the solid red line are unphysical due to the lightest stau becoming the LSP. The present discrepancy stands at $34(11) \times 10^{-10}$ with the above plots showing 1 and 2 σcontours.

4.1 Muon $g-2$

Figure 2, shows contour plots for the SUSY contributions towards the muon $g-2$. Both minimum A and minimum B (upper and lower plots respectively) give good fits to the present discrepancy between experiment and Standard Model prediction. As expected, a larger contribution to the muon $g-2$ is obtained in the lower left corner of the $(m_F, M_{1/2})$ plane where the SUSY spectrum is lightest and decreases as we move towards a heavier spectrum in the top right corner. It is also clear that for any one point in the $(m_F, M_{1/2})$ plane, minimum B gives a larger contribution than the corresponding point in minimum A. This relative enhancement can be ascribed to the dominant chargino-sneutrino diagram via the presence of a lighter muon sneutrino for the case of minimum B, as can be seen in figure 3.

The present muon $g-2$ discrepancy lies at 34×10^{-10} but over the past 12 months it has varied from a 1.5σ to 3σ effect. Also the size of the present discrepancy depends on

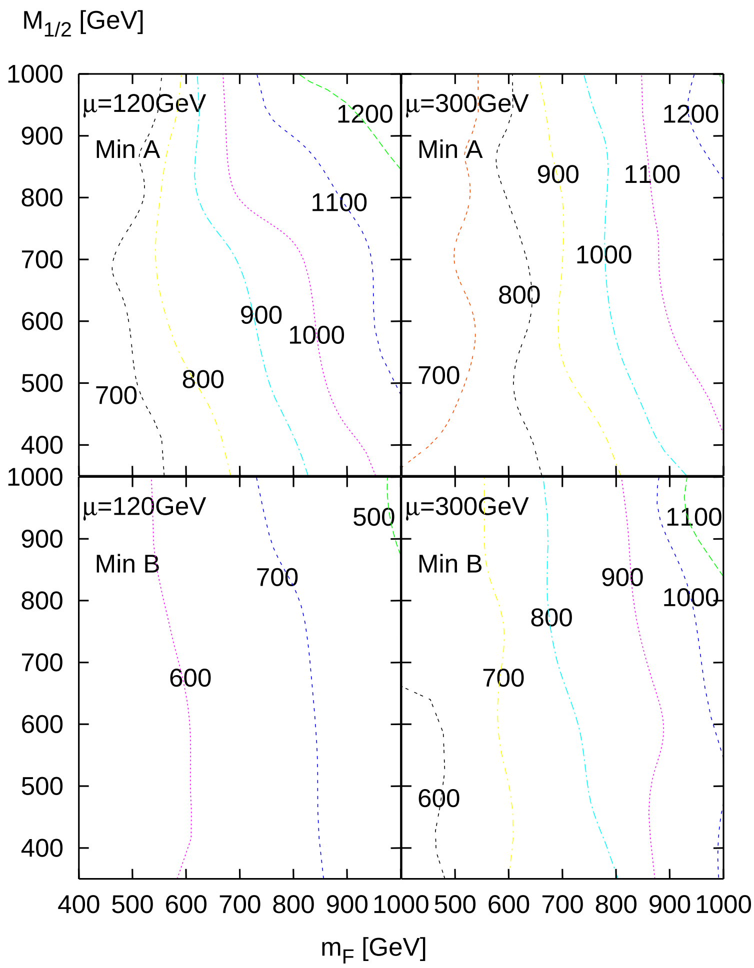

Figure 3: Contours of the second generation sneutrino mass, $m_{\tilde{\nu}_\mu}$, are plotted in the plane of $(m_F, M_{1/2})$. The contours are in the units of GeV. The four plots, are obtained from the two minima, minimum A and minimum B with $\mu = 120$ and 300 GeV as labelled. All points in the top left corner with approximately $M_{1/2} > 700$ GeV and $m_F > 700$ GeV are unphysical due to the lightest stau becoming the LSP.

the experimental data used in the calculation of the Standard model prediction. The value we have used throughout our analysis [23] makes use of e^+e^- data. On the other hand it is possible to do the same calculation making use if τ decay data [24], which gives a lower discrepancy of 9.4×10^{-10}. As a result we think it worth while looking into how our best fit regions would change if a lower discrepancy was assumed. For simplicity we took 3 points in the $(m_F, M_{1/2})$ plane of minimum A with $\mu = 120$ GeV and gradually changed the $g-2$ discrepancy from 34×10^{-10} down to 0. The results are presented in figure 4 as a plot of χ^2 against the muon $g-2$ discrepancy, a_μ^{New}.

With the discrepancy held at 34×10^{-10} the best fit point is near $M_{1/2} = 450$ GeV and $m_F = 550$ GeV. Following the curve corresponding to this point in parameter space, we can see that as the muon $g-2$ discrepancy is lowered the χ^2 gradually increased. Therefore the best fit point has moved in the positive $M_{1/2}$, m_F direction. Looking at

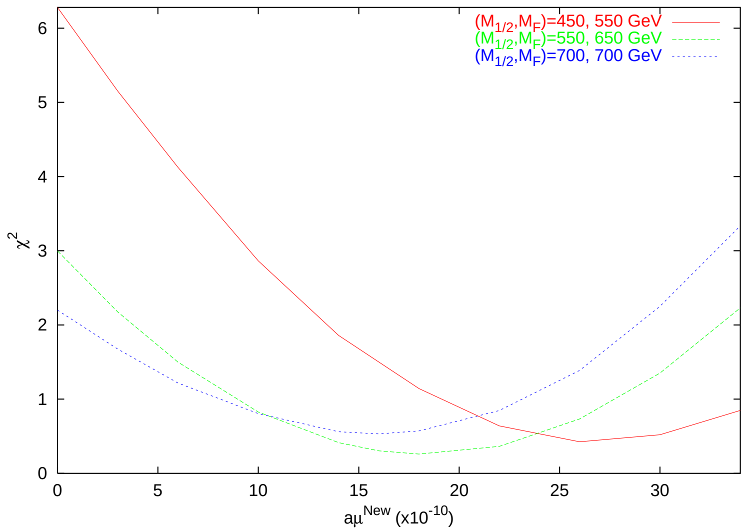

Figure 4: This plot displays the effect on χ^2 due to a future change in the value of the muon $g-2$ discrepancy. The value of the muon anomalous magnetic moment is varied from the present value of 34×10^{-10} down to zero. The resulting change in χ^2 is observed for three points in the $(m_F, M_{1/2})$ plane.

the two further curves in figure 4 we can see that if $a_\mu^{\mathrm{New}} \sim 16 \times 10^{-10}$ then the best fit point would move nearer $M_{1/2} = 550\,\mathrm{GeV}$ and $m_F = 650\,\mathrm{GeV}$. One particular point of interest is $a_\mu^{\mathrm{New}} = 9.4 \times 10^{-10}$, the value for the discrepancy as given by the Standard Model prediction from τ decay data. If we make an approximation, based on the curves in figure 4, we can say that the best fit point, for $a_\mu^{\mathrm{New}} = 9.4 \times 10^{-10}$, would be in the region $M_{1/2} = 550 - 700\,\mathrm{GeV}$, $m_F = 650 - 700\,\mathrm{GeV}$.

4.2 $\tau \to \mu\gamma$

Figure 5 displays contours for the quantity BR$(\tau \to \mu\gamma)$ for both minima with $\mu = 120$ and $300\,\mathrm{GeV}$ as labelled. The general pattern of the contours show larger branching ratio for lighter SUSY spectrum and smaller branching ratio for heavier spectrum. This pattern is not strictly obeyed in the bottom left panel which shows results for minimum B with $\mu = 120\,\mathrm{GeV}$. The reason for this is that our numerical procedure adds a large penalty χ^2 contribution for a $\tau \to \mu\gamma$ branching ratio larger than the BaBar limit of 2.0×10^{-6}. Looking at the bottom left panel in figure 5 we would expect the branching ratio to exceed the present limit as we go to a lighter spectrum. The result of adding this penalty χ^2 is to numerically force an alternative solution to be found which gives lower branching ratio and disrupts the pattern. Recalculation of this region of parameter space without the additional χ^2 penalty does indeed yield values of BR$(\tau \to \mu\gamma)$ as large as 6.0×10^{-6}, these points would therefore follow the expected contour pattern but are clearly experimentally excluded.

Looking at figure 5, the branching ratio for minimum A with $\mu = 120$ and $300\,\mathrm{GeV}$ is well below the present experimental bound. On the other hand, the branching ratio for minimum B, with $\mu = 120\,\mathrm{GeV}$ figure 5, is right at the present 90% confidence level bound

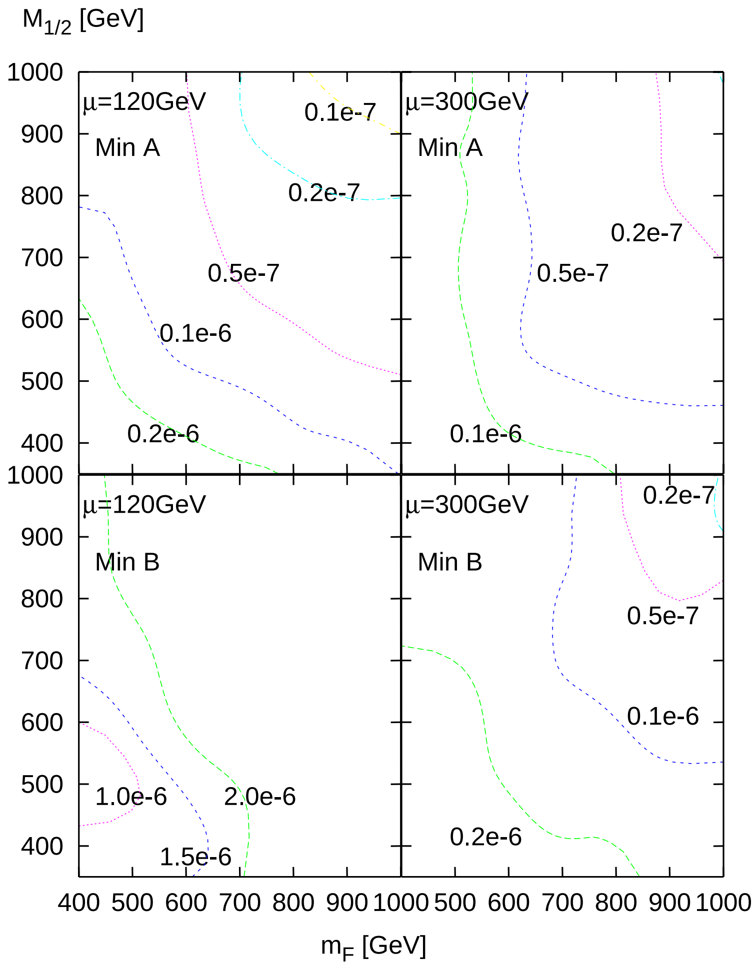

Figure 5: Contours of $BR(\tau \to \mu\gamma)$ are plotted in the plane of $(m_F, M_{1/2})$. The four plots, are obtained from the two minima, minimum A and minimum B with $\mu = 120$ and $300\,\mathrm{GeV}$ as labelled. All points in the top left corner with approximately $M_{1/2} > 700\,\mathrm{GeV}$ and $m_F > 700\,\mathrm{GeV}$ are unphysical due to the lightest stau becoming the LSP.

of 2.0×10^{-6} [25]. For $\mu = 300\,\mathrm{GeV}$ minimum B gives a branching ratio in the range, $0.1 - 0.2 \times 10^{-6}$, just below the present bound. With BaBar expected to search as far as $\mathrm{BR}(\tau \to \mu\gamma) \sim 10^{-8}$ over the next 5 years this certainly provides a means of distinguishing the two minima.

4.3 Deviations from Yukawa unification

The plots shown in figure 6 show contour lines for $r_b = Y_b/Y_\tau$ and those in figure 7, show contour lines for $r_t = Y_t/Y_\tau$ in the best fits over the $(m_F, M_{1/2})$ plane. These parameters allow the deviation of the top, bottom and tau Yukawa couplings away from unification($r_b = r_t = 1$). Both parameters show significant dependence upon m_F and weak dependence upon $M_{1/2}$, with increasing $r_{t,b}$ values as we move towards larger m_F. The plots show that the level of deviation from Yukawa unification required for a good χ^2 fit to be obtained is of the order of 20-35% in r_b and 0-10% in r_t. It is possible to account for

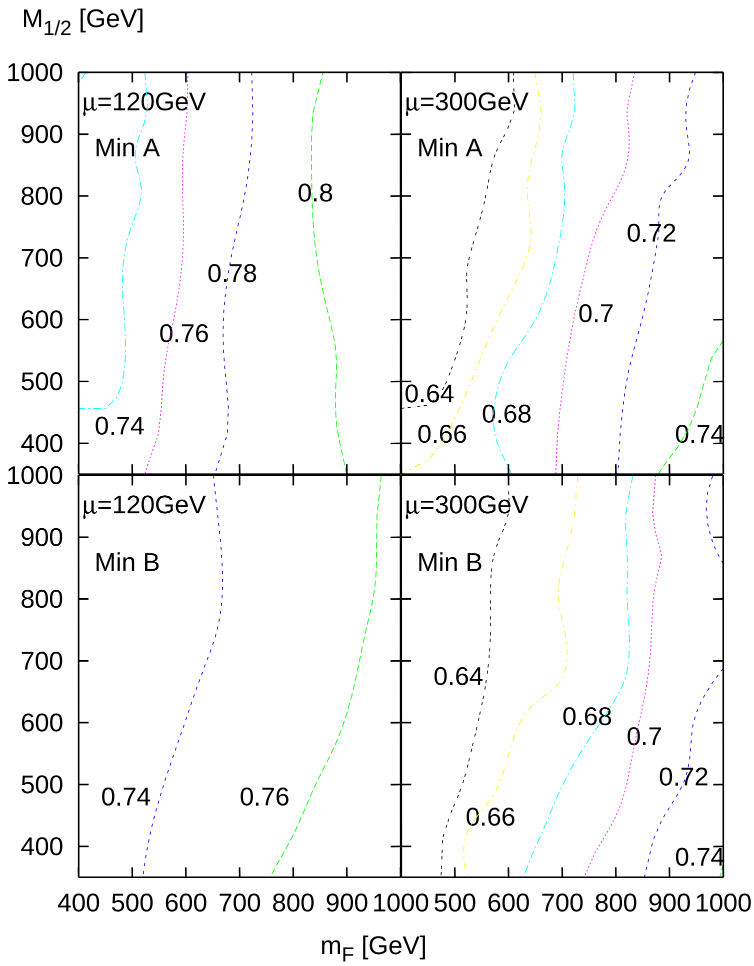

Figure 6: Contours of $r_b = Y_b/Y_\tau$ are plotted in the plane of $(m_F, M_{1/2})$. The four plots, are obtained from the two minima, minimum A and minimum B with $\mu = 120$ and $300\,\mathrm{GeV}$ as labelled. All points in the top left corner with approximately $M_{1/2} > 700\,\mathrm{GeV}$ and $m_F > 700\,\mathrm{GeV}$ are unphysical due to the lightest stau becoming the LSP.

this level of deviation through the presence of subleading operators, of the type mentioned in eq. (2.14), in the 33 element of the Yukawa matrices. Hence the 33 element in eq. (2.13) should read,

$$Y_{33} = a_{33} + \mathcal{O} + \mathcal{O}' + \cdots \tag{4.2}$$

where the operators $\mathcal{O}$ and $\mathcal{O}'$ are responsible for generating $r_{t,b} \neq 1$. The 23 block of the neutrino Yukawa matrix has already shown us that a contribution to the Yukawa matrices from a subleading operator can actually be comparable to those from a leading operator. This occurs in the 23 element of the neutrino Yukawa matrix, where there is a contribution from the operator $\mathcal{O}^I$ and the neutrino matrix is the only one that receives a non-zero Clebsch as can be seen in table 1. This leads to the relative sizes of the elements $Y_{\nu\,23} \sim 0.44$ and $Y_{\nu\,33} \sim 1$. A similar subleading contribution to the 33 element of the up and down quark Yukawa matrices could easily account for a deviation from third family Yukawa unification at the level discovered in our study.

JHEP05(2003)016

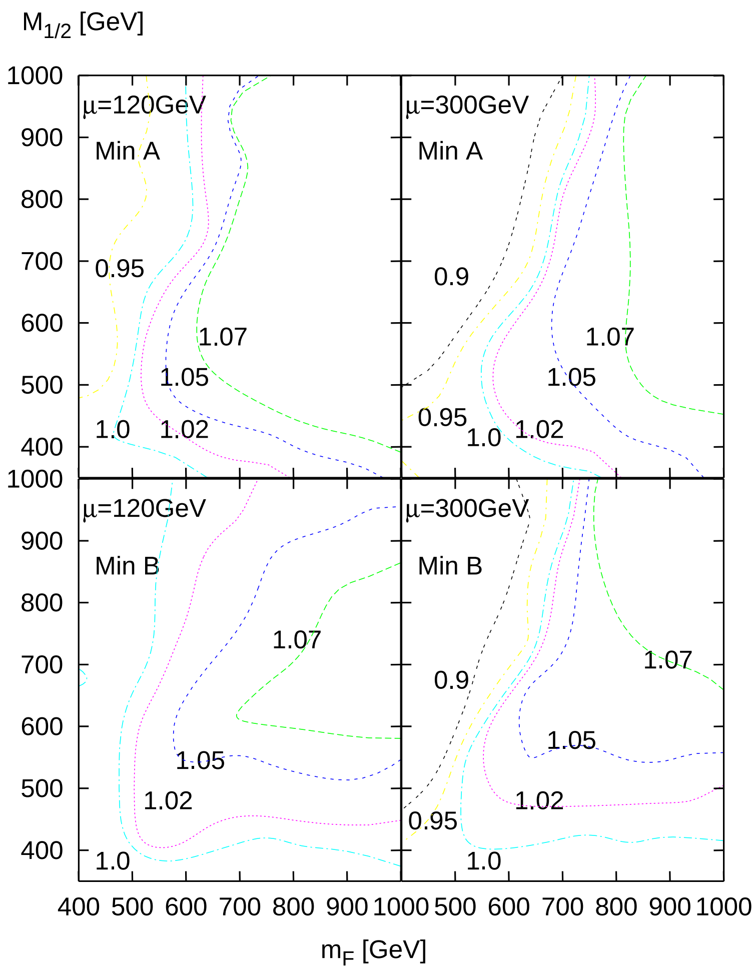

Figure 7: Contours of $r_t = Y_t/Y_\tau$ are plotted in the plane of $(m_F, M_{1/2})$. The four plots, are obtained from the two minima, minimum A and minimum B with $\mu = 120$ and 300 GeV as labelled. All points in the top left corner with approximately $M_{1/2} > 700$ GeV and $m_F > 700$ GeV are unphysical due to the lightest stau becoming the LSP.

Here we do not study the region in the parameter space $m_F > 2$ TeV, $A_0 \approx -2\,m_F$ where the exact unification might work [26]. Instead, we carried out a study of the additional χ^2 penalty incurred due to demanding exact Yukawa unification in the region $m_F < 2$ TeV and $A_0 = 0$. Figure 8 shows the result as χ^2 contour plots in the $r_t - r_b$ plane corresponding to the best fits. The three panels were obtained from three points in the $(m_F, M_{1/2})$ plane and show that a very heavy penalty $\delta\chi^2 > 10$ is paid when requiring exact Yukawa unification in this SUSY region.

4.4 Future Higgs searches

Figure 9 shows mass contours of the CP odd pseudoscalar Higgs, m_{A^0}. These plots show that for the Pseudoscalar Higgs mass minimum A prefers values approximately $200 - 300$ GeV lower than minimum B. In figure 9 we see that for both $\mu = 120$ and 300 GeV, minimum A gives a very light pseudoscalar Higgs mass, $m_{A^0} \sim 108$ GeV, in the

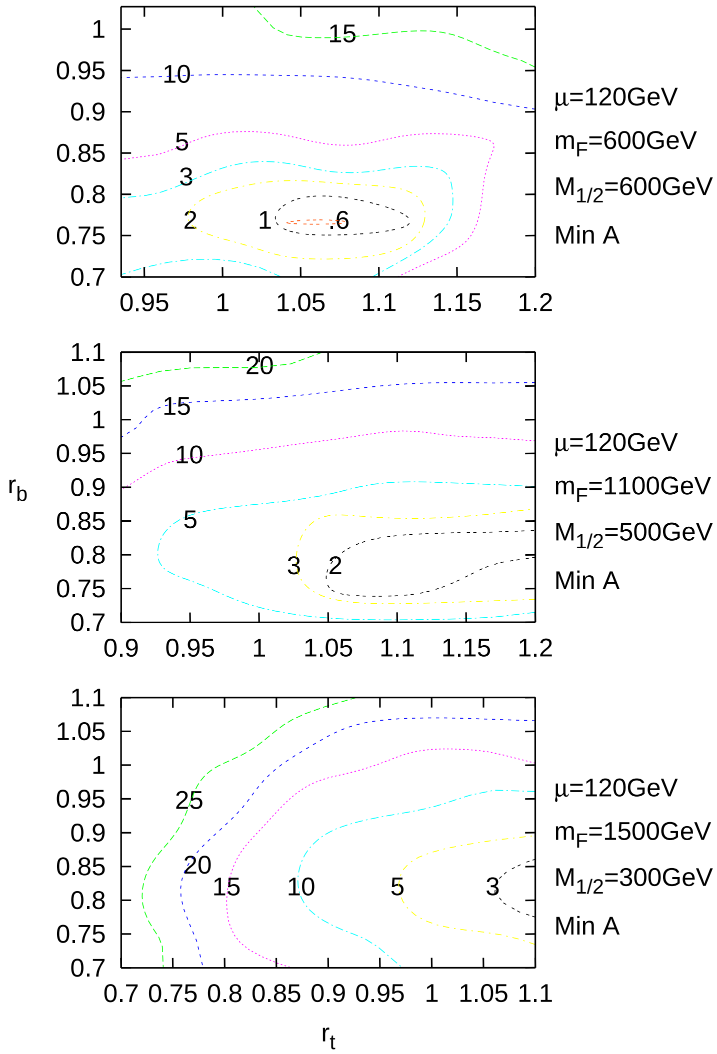

Figure 8: χ^2 contours in the $r_t - r_b$ plane. The plots are generated with $\mu = 120\,\mathrm{GeV}$ and for minimum A. The three plots are each generated with fixed $M_{1/2}$, m_F as labelled. The plots display the χ^2 penalty which is required for exact Yukawa unification to be achieved.

low $M_{1/2}$, m_F region. This is in fact the same region in which minimum A provides its lowest χ^2. In fact table 4 shows that for the best fit point in minimum A we have a pseudoscalar mass of 102 GeV and a light CP even mass of 106 GeV. With the Tevatron now taking data there is a high probability that the present lower bound on Higgs masses will be pushed higher. Hence we have undertaken a study of the effect this would have on our best fits. The plot in figure 10 shows the increase in χ^2, for four points in the $(m_F, M_{1/2})$ plane of minimum A, due to an increase in the lower bound on the Higgs masses m_{A^0}, m_{h^0}. It clearly shows that all four of the points can accommodate an increase in the lower bound up to approximately 120 GeV, above this the χ^2 increases sharply due the inability to accommodate such a large lower bound.

The coupling of the light CP even Higgs, h^0, to the Z boson is proportional to $\sin(\beta-\alpha)$ and that of the heavy CP even Higgs, H^0, is proportional to $\cos(\beta-\alpha)$, where α is the

JHEP05(2003)016

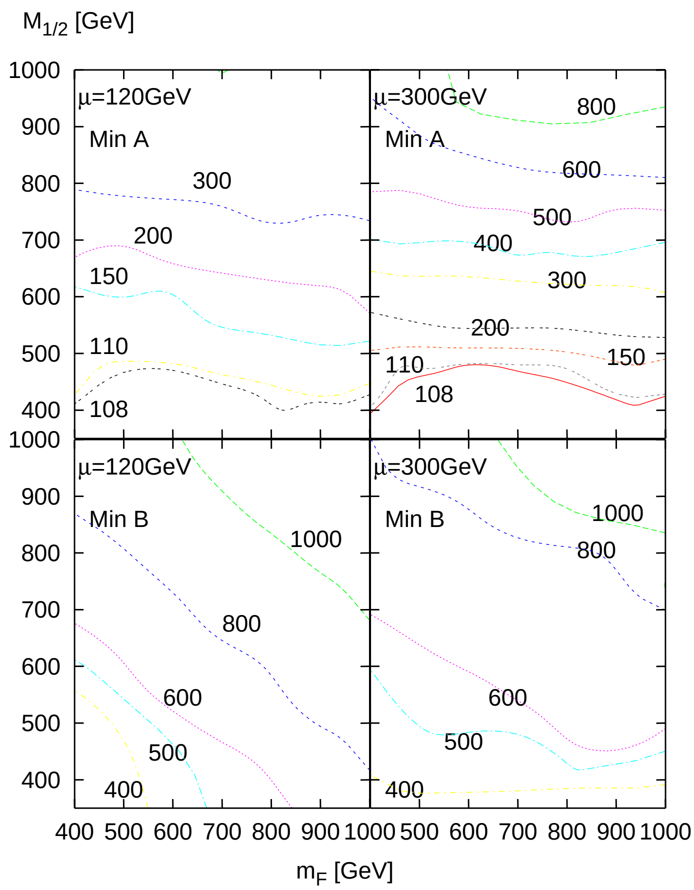

Figure 9: Contours of the CP odd Pseudoscalar Higgs mass, m_{A^0}, are plotted in the plane of $(m_F, M_{1/2})$. The contours are in the units of GeV. The four plots, are obtained from the two minima, minimum A and minimum B with $\mu = 120$ and 300 GeV as labelled. All points in the top left corner with approximately $M_{1/2} > 700$ GeV and $m_F > 700$ GeV are unphysical due to the lightest stau becoming the LSP.

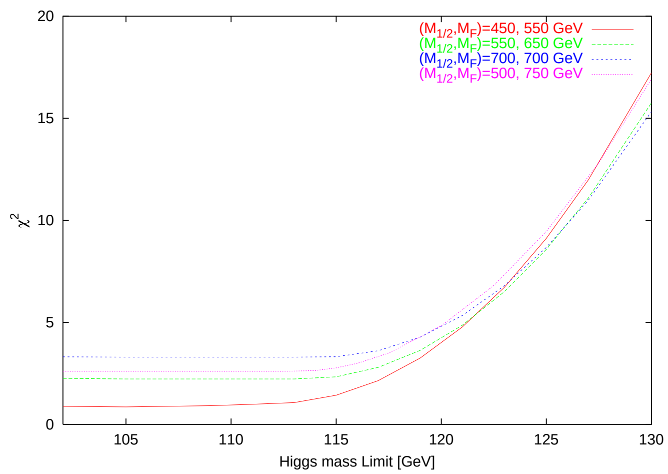

Figure 10: This plot displays the effect on χ^2 due to an increase in the lower bound on the Higgs mass from direct searches. As in figure 4 the variation in χ^2 is observed through individual points in the $(m_F, M_{1/2})$ plane.

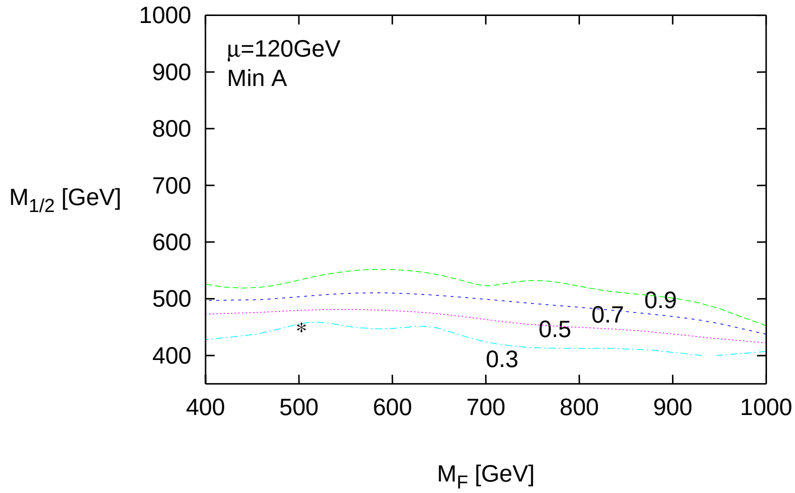

Figure 11: Contours of $\sin(\beta-\alpha)$, which defines the strength of the Z boson coupling to the Higgs h^0 relative to that of H^0. For values of $\sin(\beta-\alpha)$ near one the $Z-h^0$ coupling is large and for small values the $Z-H^0$ coupling is large. The contours are plotted using data from minimum A with $\mu = 120\,\text{GeV}$. The the best fit point at $M_{1/2} = 450\,\text{GeV}$, $m_f = 500\,\text{GeV}$ is marked with an asterisk.

mixing angle for the CP even Higgs states. In figure 11, which shows contours of $\sin(\beta-\alpha)$ for points in minimum A, we see that in the low $M_{1/2}$ region $\sin(\beta-\alpha)$ is small and hence the Z couples dominantly to the heavier Higgs state H^0, rather that the lighter h^0. Therefore, in this region it is the heavier state, H^0, which is the standard model like Higgs and so the LEP limit will apply to the larger m_{H^0} and not m_{h^0}. Table 4 shows that we have exactly this situation for the best fit points of minimum A where $\sin(\beta-\alpha) \sim 0.2$, therefore the standard model like Higgs is the heavier state H^0 for these points with a mass of 113 GeV. Assuming a 3 GeV error in our numerical calculation means we are compatible with the present LEP limit of 114.4 GeV.

We have checked that the light Higgs spectrum is consistent with the current limit on the rate for $B_s \to \mu^+\mu^-$. [22]

4.5 CHOOZ angle, θ_{13}

Figure 12 shows scatter plots of $\sin^2 2\theta_{13}$ against Δm^2_{Atm} for both minimum A and minimum B with $\mu = 120$ and 300 GeV. Each point denotes values obtained from individual points in the $(m_F, M_{1/2})$ plane, with points grouped according to the value of χ^2. These plots show that the Model can easily yield values of θ_{13} that are within the present CHOOZ limit, $\theta_{13} \lesssim 0.22$. Each of the plots in figure 12 shows that the best fit points, denoted by a + symbol, give a range of values of $\sin^2 2\theta_{13}$ from, 10^{-6} to 0.1. Although our results do not give any firm prediction for the value of θ_{13}, it can be seen that the model favours the region, $10^{-4} < \sin\theta_{13} < 0.1$, just below the present CHOOZ limit.

5. Summary and conclusion

We have performed a complete global phenomenological analysis of a realistic string-inspired model based on the supersymmetric Pati-Salam $SU(4) \times SU(2)_L \times SU(2)_R$ gauge

JHEP05(2003)016

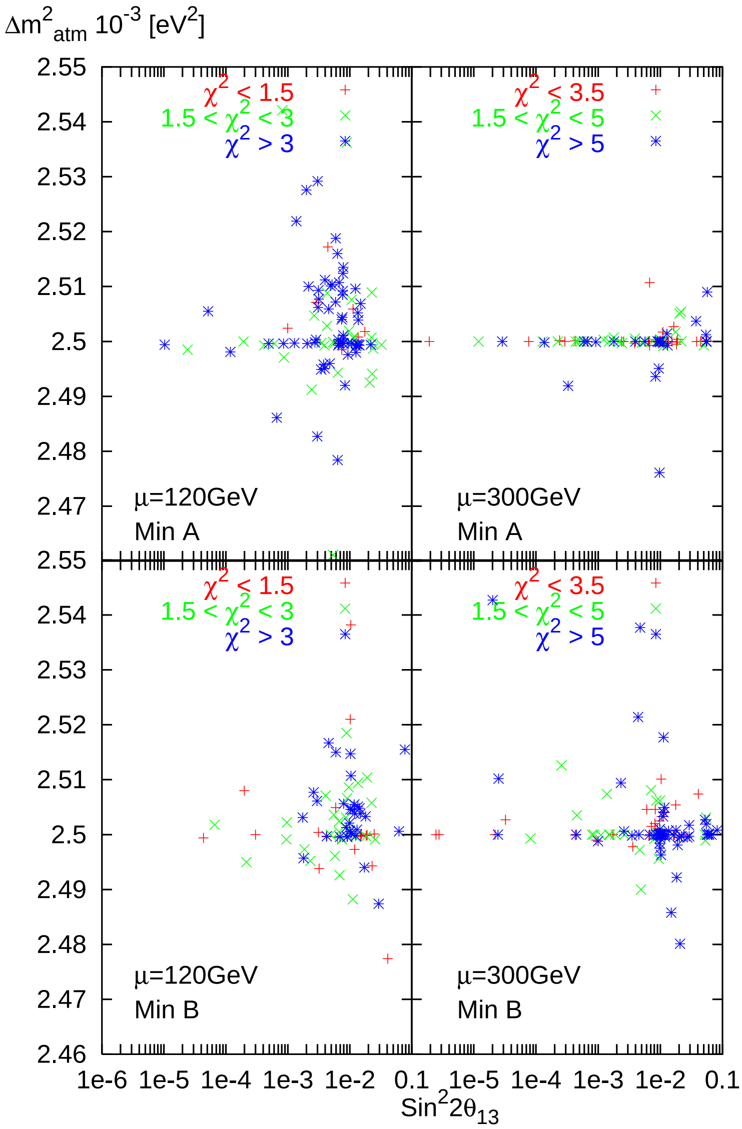

Figure 12: The four panels contain scatter plots of the values of Δm^2_{Atm} against $\sin^2 2\theta_{13}$ coming from the best fit points in the $(m_F, M_{1/2})$ plane. Each plot shows results obtained from either minimum A or minimum B, with $\mu = 120$ or 300 GeV as labelled. The points are grouped according to their χ^2 values as inticated.

group supplemented by a U(1) family symmetry. Global contour plots in the $(m_F, M_{1/2})$ plane have been presented in figure 1, showing two χ^2 minima. These two distinct minima differ numerically by the relative sign of the D-term. This gives interesting phenomenological differences between the two minima, notably one has $BR(\tau \to \mu\gamma)$ near the present limit and a heavy pseudoscalar Higgs m_{A^0}, while the other has $BR(\tau \to \mu\gamma)$ well below the present bound but a light pseudoscalar Higgs m_{A^0}. Both minima give a good fit to the present muon $g - 2$ discrepancy over a large region of parameter space and give $\sin^2 2\theta_{13}$ over the range $10^{-5} - 0.1$. Our best fit predictions for the superpartner masses for each of the two minima for two different μ values are summarised in table 4.

We emphasise again that our analysis really should be considered as consisting of two distinct parts, associated with flavour physics on the one hand and unification and electroweak symmetry breaking on the other hand. For the flavour part, we have proposed a complete model in table 1 which gives an accurate description of all fermion masses and mixing angles, including the LMA MSW neutrino solution. We have shown that improved limits on $BR(\tau \to \mu\gamma)$ could begin to rule out one of our two minima. The conclusions on $BR(\tau \to \mu\gamma)$ are applicable to a wide class of models which achieve approximate maximal atmospheric neutrino mixing via the see-saw mechanism in the MSSM with a large 23 entry in the neutrino Yukawa matrix. On the other hand $BR(\mu \to e\gamma)$ is predicted to be about two orders of magnitude below the current limit, which is a consequence of the specific flavour structure of the model in table 1.

Regarding unification, the model predicts approximate third family Yukawa unification and hence large $\tan\beta \sim 50$. Electroweak symmetry breaking was achieved with the help of D-terms and non-universal soft Higgs mass, which allows small μ values. The property of exact Yukawa unification was relaxed throughout the analysis and it was found that a deviation of 20-35% for the bottom Yukawa coupling and 0-10% for the top Yukawa coupling are required for a good fit to be obtained. We showed that relaxing Yukawa unification has the effect of allowing small values of the soft scalar mass m_F, and lighter squark and slepton masses as a consequence.

Further studies of the effects of future direct Higgs searches and a change to the present muon $g-2$ discrepancy are shown in figures 4 and 10. We found that our best fit points, for the minima with lighter Higgs masses, can accommodate a lower bound on Higgs masses up to about 120 GeV. For these points the coupling of the lighter CP even Higgs state to the Z boson is suppressed, leaving the heavier of the two CP even states acting as the standard model like Higgs.

In conclusion, we have constructed and analysed a complete supersymmetric Pati-Salam model which agrees with all laboratory observables and constraints. Using a global analysis we identify the most preferred regions of the SUSY parameter space, and find a rather light superpartner spectrum corresponding to $(m_F, M_{1/2}) \sim (600, 600)$ (in GeV) well within reach of the LHC.

Acknowledgments

S.K. thanks PPARC for a Senior Fellowship and J.P. thanks PPARC for a studentship.

References

[1] Super-Kamiokande collaboration, Y. Fukuda et al., *Measurement of a small atmospheric ν_μ/ν_e ratio*, *Phys. Lett.* **B 433** (1998) 9 [hep-ex/9803006]; *Study of the atmospheric neutrino flux in the multi-GeV energy range*, *Phys. Lett.* **B 436** (1998) 33 [hep-ex/9805006]; *Evidence for oscillation of atmospheric neutrinos*, *Phys. Rev. Lett.* **81** (1998) 1562 [hep-ex/9807003].

[2] SNO collaboration, Q.R. Ahmad et al., *Direct evidence for neutrino flavor transformation from neutral-current interactions in the Sudbury Neutrino Observatory*, *Phys. Rev. Lett.* **89** (2002) 011301 [nucl-ex/0204008];

SNO collaboration, Q.R. Ahmad et al., *Measurement of day and night neutrino energy spectra at SNO and constraints on neutrino mixing parameters*, *Phys. Rev. Lett.* **89** (2002) 011302 [nucl-ex/0204009].

[3] KamLAND collaboration, K. Eguchi et al., *First results from KamLAND: evidence for reactor anti-neutrino disappearance*, *Phys. Rev. Lett.* **90** (2003) 021802 [hep-ex/0212021].

[4] G.L. Fogli, E. Lisi, A. Marrone, D. Montanino, A. Palazzo and A.M. Rotunno, *Solar neutrino oscillation parameters after first kamland results*, *Phys. Rev.* **D 67** (2003) 073002 [hep-ph/0212127];
P.C. de Holanda and A.Y. Smirnov, *LMA MSW solution of the solar neutrino problem and first kamland results*, *J. Cosmol. Atrop. Phys.* **0302** (2003) 001 [hep-ph/0212270];
V. Barger and D. Marfatia, *KamLAND and solar neutrino data eliminate the low solution*, *Phys. Lett.* **B 555** (2003) 144 [hep-ph/0212126];
A. Bandyopadhyay, S. Choubey, R. Gandhi, S. Goswami and D.P. Roy, *The solar neutrino problem after the first results from KamLAND*, *Phys. Lett.* **B 559** (2003) 121 [hep-ph/0212146];
M. Maltoni, T. Schwetz and J.W.F. Valle, *Combining first KamLAND results with solar neutrino data*, hep-ph/0212129.

[5] S.F. King, *Atmospheric and solar neutrinos with a heavy singlet*, *Phys. Lett.* **B 439** (1998) 350 [hep-ph/9806440];
S.F. King, *Atmospheric and solar neutrinos from single right-handed neutrino dominance and* U(1) *family symmetry*, *Nucl. Phys.* **B 562** (1999) 57 [hep-ph/9904210];
S.F. King, *Large mixing angle msw and atmospheric neutrinos from single right-handed neutrino dominance and* U(1) *family symmetry*, *Nucl. Phys.* **B 576** (2000) 85 [hep-ph/9912492].

[6] J.C. Pati and A. Salam, *Lepton number as the fourth color*, *Phys. Rev.* **D 10** (1974) 275.

[7] I. Antoniadis and G.K. Leontaris, *A supersymmetric* $SU(4) \times O(4)$ *model*, *Phys. Lett.* **B 216** (1989) 333;
I. Antoniadis, G.K. Leontaris and J. Rizos, *A three generation* $SU(4) \times O(4)$ *string model*, *Phys. Lett.* **B 245** (1990) 161.

[8] G. Shiu and S.H.H. Tye, *TeV scale superstring and extra dimensions*, *Phys. Rev.* **D 58** (1998) 106007 [hep-th/9805157];
L.L. Everett, G.L. Kane, S.F. King, S. Rigolin and L.-T. Wang, *Supersymmetric Pati-Salam models from intersecting D-branes*, *Phys. Lett.* **B 531** (2002) 263 [hep-ph/0202100].

[9] S.F. King and M. Oliveira, *Lepton flavor violation in string inspired models*, *Phys. Rev.* **D 60** (1999) 035003 [hep-ph/9804283].

[10] S.F. King and M. Oliveira, *Neutrino masses and mixing angles in a realistic string-inspired model*, *Phys. Rev.* **D 63** (2001) 095004 [hep-ph/0009287].

[11] T. Blažek and S.F. King, *Muon anomalous magnetic moment and* $\tau \to \mu\gamma$ *in a realistic string-inspired model of neutrino masses*, *Phys. Lett.* **B 518** (2001) 109 [hep-ph/0105005].

[12] S.F. King and M. Oliveira, *Yukawa unification as a window into the soft supersymmetry breaking lagrangian*, *Phys. Rev.* **D 63** (2001) 015010 [hep-ph/0008183].

[13] M.E. Gomez, G. Lazarides and C. Pallis, *Yukawa quasi-unification*, *Nucl. Phys.* **B 638** (2002) 165 [hep-ph/0203131].

[14] M.E. Gomez, G. Lazarides and C. Pallis, *On Yukawa quasi-unification with $\mu < 0$*, *Phys. Rev.* **D 67** (2003) 097701 [hep-ph/0301064].

[15] CDF collaboration, T. Affolder et al., *Search for neutral supersymmetric Higgs bosons in $p\bar{p}$ collisions at $\sqrt{s} = 1.8$ TeV*, *Phys. Rev. Lett.* **86** (2001) 4472 [hep-ex/0010052].

[16] S.F. King, $\mathrm{SU}(4) \times \mathrm{SU}(2)_L \times \mathrm{SU}(2)_R$ *as a surrogate SUSY GUT*, *Phys. Lett.* **B 325** (1994) 129, erratum *ibid.* **B325** (1994) 538;
B.C. Allanach and S.F. King, *Fermion masses in a supersymmetric* $\mathrm{SU}(4) \times \mathrm{SU}(2)_L \times \mathrm{SU}(2)_R$ *model*, *Nucl. Phys.* **B 456** (1995) 57 [hep-ph/9502219];
B.C. Allanach and S.F. King, *Neutrino masses and mixing angles in a supersymmetric* $\mathrm{SU}(4) \otimes \mathrm{SU}(2)_L \otimes \mathrm{SU}(2)_R$ *model*, *Nucl. Phys.* **B 459** (1996) 75 [hep-ph/9509205];
B.C. Allanach, S.F. King, G.K. Leontaris and S. Lola, *A new approach to Yukawa textures in supersymmetric unified models with gauged family symmetries*, *Phys. Rev.* **D 56** (1997) 2632 [hep-ph/9610517].

[17] S.F. King, *Constructing the large mixing angle mns matrix in see-saw models with right-handed neutrino dominance*, *J. High Energy Phys.* **09** (2002) 011 [hep-ph/0204360].

[18] T. Blažek and S.F. King, *Lepton flavour violation in the constrained MSSM with natural neutrino mass hierarchy*, hep-ph/0211368.

[19] T. Blažek, M. Carena, S. Raby and C.E.M. Wagner, *A global χ^2 analysis of electroweak data in* SO(10) *SUSY GUTs*, *Phys. Rev.* **D 56** (1997) 6919 [hep-ph/9611217].

[20] M. Carena, J.R. Espinosa, M. Quiros and C.E.M. Wagner, *Analytical expressions for radiatively corrected Higgs masses and couplings in the MSSM*, *Phys. Lett.* **B 355** (1995) 209 [hep-ph/9504316];
M. Carena, M. Quiros and C.E.M. Wagner, *Effective potential methods and the Higgs mass spectrum in the MSSM*, *Nucl. Phys.* **B 461** (1996) 407 [hep-ph/9508343];
J.A. Casas, J.R. Espinosa, M. Quiros and A. Riotto, *The lightest Higgs boson mass in the minimal supersymmetric standard model*, *Nucl. Phys.* **B 436** (1995) 3 [hep-ph/9407389].

[21] R. Hempfling, *Yukawa coupling unification with supersymmetric threshold corrections*, *Phys. Rev.* **D 49** (1994) 6168;
L.J. Hall, R. Rattazzi and U. Sarid, *The top quark mass in supersymmetric* SO*(10) unification*, *Phys. Rev.* **D 50** (1994) 7048 [hep-ph/9306309];
M. Carena, M. Olechowski, S. Pokorski and C.E.M. Wagner, *Electroweak symmetry breaking and bottom-top Yukawa unification*, *Nucl. Phys.* **B 426** (1994) 269 [hep-ph/9402253];
T. Blažek, S. Raby and S. Pokorski, *Finite supersymmetric threshold corrections to CKM matrix elements in the large* $\tan\beta$ *regime*, *Phys. Rev.* **D 52** (1995) 4151 [hep-ph/9504364].

[22] A. Dedes, H.K. Dreiner, U. Nierste and P. Richardson, *Trilepton events and $B_s \to \mu^+\mu^-$: no-lose for MSUGRA at the Tevatron?*, hep-ph/0207026;
CDF collaboration and D0 collaboration, T. Kamon, *Prospects of discovery for supersymmetry at the Tevatron*, talk given at *10th international conference on supersymmetry and unification of fundamental interactions (SUSY02)*, Hamburg, Germany, 17-23 Jun 2002, hep-ex/0301019.

[23] K. Hagiwara, A.D. Martin, D. Nomura and T. Teubner, *The SM prediction of $g-2$ of the muon*, *Phys. Lett.* **B 557** (2003) 69 [hep-ph/0209187];
M. Davier, S. Eidelman, A. Hocker and Z. Zhang, *Confronting spectral functions from e^+e^- annihilation and tau decays: consequences for the muon magnetic moment*, *Eur. Phys. J.* **C 27** (2003) 497 [hep-ph/0208177];

JHEP05(2003)016

A. Hoefer, J. Gluza and F. Jegerlehner, *Pion pair production with higher order radiative corrections in low energy* e^+e^- *collisions*, *Eur. Phys. J.* **C 24** (2002) 51 [hep-ph/0107154];
B.V. Geshkenbein, *The more precise determination of hadronic contribution to muonic* $(g-2)$ *factor and to* $\alpha(m_z^2)$, hep-ph/0301265.

[24] M. Davier, S. Eidelman, A. Hocker and Z. Zhang, *Confronting spectral functions from* e^+e^- *annihilation and tau decays: consequences for the muon magnetic moment*, *Eur. Phys. J.* **C 27** (2003) 497 [hep-ph/0208177].

[25] BABAR collaboration, C. Brown, *Search for the lepton number violating decay* $\tau \to \mu\gamma$, *eConf* **C0209101** (2002) TU12 [hep-ex/0212009].

[26] T. Blažek, R. Dermíšek and S. Raby, *Predictions for Higgs and supersymmetry spectra from* SO(10) *Yukawa unification with* $\mu > 0$, *Phys. Rev. Lett.* **88** (2002) 111804 [hep-ph/0107097]; *Yukawa unification in* SO(10), *Phys. Rev.* **D 65** (2002) 115004 [hep-ph/0201081];
K. Tobe and J.D. Wells, *Revisiting top-bottom-tau yukawa unification in supersymmetric grand unified theories*, hep-ph/0301015;
D. Auto, H. Baer, C. Balazs, A. Belyaev, J. Ferrandis and X. Tata, *Yukawa coupling unification in supersymmetric models*, hep-ph/0302155.

JHEP05(2003)016